CHINESE OPTICS LETTERS

Vol. 19, No. 9 | September 2021

# Rare-earth ions-doped mid-infrared (2.7–3 μm) bulk lasers: a review [Invited]

Hongkun Nie (聂鸿坤)[1], Feifei Wang (王菲菲)[1], Junting Liu (刘俊亭)[1], Kejian Yang (杨克建)[1,2], Baitao Zhang (张百涛)[1,2*], and Jingliang He (何京良)[1,2]

[1] State Key Laboratory of Crystal Materials, Shandong University, Jinan 250100, China

[2] Key Laboratory of Laser & Infrared System, Ministry of Education, Shandong University, Qingdao 266237, China

*Corresponding author: btzhang@sdu.edu.cn

Received April 27, 2021 | Accepted May 21, 2021 | Posted Online August 25, 2021

Mid-infrared (MIR) laser sources operating in the 2.7–3 μm spectral region have attracted extensive attention for many applications due to the unique features of locating at the atmospheric transparency window, corresponding to the "characteristic fingerprint" spectra of several gas molecules, and strong absorption of water. Over the past two decades, significant developments have been achieved in 2.7–3 μm MIR lasers benefiting from the sustainable innovations in laser technology and the great progress in material science. Here, we mainly summarize and review the recent progress of MIR bulk laser sources based on the rare-earth ions-doped crystals in the 2.7–3 μm spectral region, including $Er^{3+}$-, $Ho^{3+}$-, and $Dy^{3+}$-doped crystalline lasers. The outlooks and challenges for future development of rare-earth-doped MIR bulk lasers are also discussed.

**Keywords:** mid-infrared laser; 2.7–3 μm spectral region; $Er^{3+}$, $Ho^{3+}$, and $Dy^{3+}$-doped crystal.
**DOI:** 10.3788/COL202119.091407

## 1. Introduction

A coherent laser source emitting mid-infrared (MIR) radiation in the 2.7–3 μm wavelength band has several unique features, including (i) locating at the well-known atmospheric transparency window[1]; (ii) corresponding to the strong rovibrational absorption lines of various gas molecules[2,3]; (iii) overlapping the strong absorption peak of water[4]. Based on the above merits, it has recently attracted tremendous attention owing to the potential applications in remote sensing, laser surgery, gas monitoring and detection, precision spectroscopy measurement, material processing and countermeasures, etc. Up to now, the most advanced MIR solid-state laser technologies that are used for 2.7–3 μm laser generation include but are not limited to the rare-earth-doped crystalline and fiber lasers[5–21], semiconductor laser diodes (LDs)[22–26], quantum cascade lasers (QCLs)[27,28], nonlinear optical frequency conversion {optical difference frequency generation (DFG)[29,30], optical parametric sources [OPSs, including optical parametric oscillators (OPOs)[31–33], optical parametric generators (OPGs)[34,35]], etc.}, and so on.

The GaIn(As)Sb/AlGaAnSb system-based strained multi-quantum-well LD is regarded as the most established semiconductor laser technology for 2–3 μm MIR laser generation[23,26], which relies on the inter-band laser transition and depends on the composition of the selected alloys. However, the Auger effect can strongly reduce the efficiency when the emitting wavelength is longer than 2 μm[26,32]. In contrast to semiconductor LDs, the laser transition in QCLs is in the conduction band, which is commonly named the inter-sub-band transition. One type of carrier and a multistage cascade scheme are the two fundamental features where QCLs differentiate from semiconductor LDs[32]. The shortest wavelength of QCLs is limited by the conduction band offset height between different heterostructure materials, while there is no fundamental limitation for the long-wavelength side. For example, the shortest wavelengths for InP- and GaAs-based QCLs are 3.4 and 8 μm, respectively. As a consequence, QCLs are more suitable for longer MIR laser generation. However, the biggest critical issue of QCLs is the large amount of dissipated heat, which makes it difficult to achieve continuous-wave (CW) laser operation at room temperature. Compared with semiconductor LDs and QCLs, converting the most mature 1 μm laser to the MIR region through nonlinear optical frequency conversion is the commonly used technique for 2.7–3 μm laser generation, especially for high-power and high-energy MIR lasers. However, either DFG or OPSs need high power and a high-beam-quality fundamental laser and a nonlinear optical convertor, which make the system very complex and with high cost. Therefore, researchers

have endeavored to pursue 2.7–3 μm MIR laser sources with the advantages of being robust and compact, high efficiency, high beam quality, low cost, being easy to use, etc.

Over the past two decades, benefiting from the great progress in material science and technology, a lot of MIR laser gain materials, especially rare-earth-doped crystalline and fiber materials with excellent optical, thermal, and mechanical properties have been developed[5–21,36–39]. Thus far, direct laser emissions in the 2.7–3 μm spectral region have become reality[9,16,21,32,40,41] and thus have the significant advantages of low cost, high efficiency, simple structure, and low loss. Direct laser emission around 2.7–3 μm is primarily based on the optical transitions offered by $Er^{3+}$-, $Ho^{3+}$-, and $Dy^{3+}$-doped gain materials. The typical emission spectrum and wavelength coverages of $Er^{3+}$-, $Ho^{3+}$-, and $Dy^{3+}$-doped lasers around 3 μm are shown in Fig. 1[19,42]. Nowadays, driven by the new materials and sustainable innovations in laser technology, a lot of crystalline and fiber lasers operating around 2.7–3 μm have been realized. Compared with fiber lasers, all solid-state lasers with bulk crystals have the main advantages of low undesirable nonlinear effects and a large mode area, which make them more suitable for generating high-energy and high-peak-power ultrashort pulses. Here, in this work, we mainly summarize and review the recent progress of MIR bulk laser sources based on the rare-earth ions-doped crystals in the 2.7–3 μm spectral region, including $Er^{3+}$-, $Ho^{3+}$-, and $Dy^{3+}$-doped all solid-state crystalline lasers.

## 2. All Solid-State Crystalline Lasers in the 2.7–3 μm Spectral Region

At present, the rare-earth ions that can achieve room temperature MIR laser operation in the 2.7–3 μm spectral region are mainly $Er^{3+}$, $Ho^{3+}$, and $Dy^{3+}$, among which the $Er^{3+}$ ion is mostly studied. Nevertheless, the MIR emission spectrum of the $Er^{3+}$ ion is a line, and the corresponding output wavelength is relatively short. In contrast, the number of electrons in the 4f shell of $Ho^{3+}$ and $Dy^{3+}$ ions is even, resulting in the Stark-level splitting being greatly influenced by the crystal fields. Thus, the fluorescence spectra of the $Ho^{3+}$ and $Dy^{3+}$ ions-doped crystals are usually smooth and broadband, which enables the tunable laser output and also expands the wavelength towards the infrared direction.

### 2.1. $Er^{3+}$-doped crystalline lasers in the 2.7–3 μm region

Besides the well-known laser transition of $^4I_{13/2} \rightarrow {}^4I_{15/2}$ emitting wavelength around 1.55 μm, the $Er^{3+}$ ion can also provide 2.7–3 μm MIR emission with the $^4I_{11/2} \rightarrow {}^4I_{13/2}$ transition. The simplified energy-level diagram of the $Er^{3+}$-doped gain medium is shown in Fig. 2(a). Easy growing and the pumping wavelength being around ~970 nm (commercial LD operation wavelength) are the two fundamental merits that make $Er^{3+}$-doped crystals much more extensively studied for the 2.7–3 μm laser generation compared to that of $Ho^{3+}$- and $Dy^{3+}$- doped crystals. As early as 1967, Robinson and Devor realized the first, to the best of our knowledge, laser oscillation of an $Er^{3+}$-doped crystalline MIR laser at 2.69 μm with a $CaF_2$:$ErF_3$ mixed crystal[43]. However, for the $Er^{3+}$:$^4I_{11/2} \rightarrow {}^4I_{13/2}$ transition, there is a so-called self-terminated effect leading to a population bottleneck issue caused by the lifetime of the upper laser level ($^4I_{11/2}$) being much shorter than that of the lower level ($^4I_{13/2}$)[44,45], which is the main obstacle preventing the development of $Er^{3+}$-doped 2.7–3 μm crystalline lasers. Up to now, several approaches have been developed to solve this detrimental feature. One is increasing the doping concentration of the $Er^{3+}$ ion to generate the "quenching effect", which could decrease the lifetime of $Er^{3+}$:$^4I_{13/2}$ so as to relieve the self-terminating behavior[11,46–49]. The energy-transfer up-conversion (ETU) process between $Er^{3+}$ and $Er^{3+}$ ions in highly doped crystals can also effectively depopulate $Er^{3+}$:$^4I_{13/2}$ to solve the population bottleneck issue. But, it should be noticed that it is a double-edged sword because of the severe thermal effects and the lifetime reduction of the upper laser level $Er^{3+}$:$^4I_{11/2}$. Another approach is co-doping with sensitized ions (typically $Yb^{3+}$) with the efficient population of $Er^{3+}$:$^4I_{11/2}$ or deactivated ions (typically $Pr^{3+}$) with efficient depopulation of $Er^{3+}$:$^4I_{13/2}$ for establishing and sustaining population inversion, as shown in Fig. 2(a)[50–60]. Besides, the

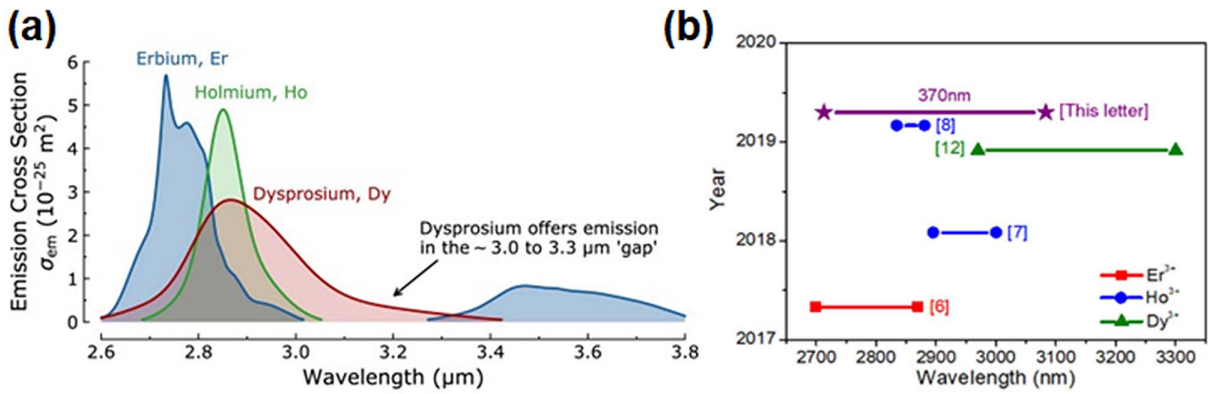


**Fig. 1.** (a) Typical emission spectrum[42] and (b) wavelength coverages[19] of $Er^{3+}$-, $Ho^{3+}$-, and $Dy^{3+}$-doped lasers.

host material is another essential factor for the $Er^{3+}$:$^4I_{11/2} \rightarrow {}^4I_{13/2}$ transition, which should have low photon energy, high radiative emission rate, and low absorption in the 2.7–3 μm band. To date, the oxide [primarily the garnet structure: $Y_3Al_5O_{12}$ (YAG), $Gd_3Ga_5O_{12}$ (GGG), $Gd_3Sc_2Ga_3O_{12}$ (GSGG), $Y_3Sc_2Ga_3O_{12}$ (YSGG), etc. and $YAlO_3$ (YAP)][11,46,50,60–67], fluoride [$CaF_2$, $SrF_2$, $LiYF_4$, $LiLuF_4$ (LLF), etc.][15,43,48,55,58,68–74], and sesquioxide crystals ($Sc_2O_3$, $Lu_2O_3$, $Y_2O_3$, etc.)[49,75–79] or ceramics have been proved to be the promising and most spread host materials for $Er^{3+}$-doped 2.7–3 μm crystalline lasers by considering the thermal conductivity, opto-mechanical properties, photon energy, etc. Moreover, the cascading laser operation of $^4I_{13/2} \rightarrow {}^4I_{15/2}$ and $^4I_{11/2} \rightarrow {}^4I_{13/2}$ transitions is another way to suppress the saturation of the $^4I_{11/2} \rightarrow {}^4I_{13/2}$ transition. Such cascade oscillation was demonstrated for instance in Er:$YLiF_4$ (YLF) Q-switched lasers and Er-doped fluoride fiber lasers[80,81].

After the first, to the best of our knowledge, realization of an $Er^{3+}$:$CaF_2$:$ErF_3$ mixed crystal operating at 2.69 μm in 1969, efficient operations both in the CW and pulsed regimes with $Er^{3+}$-doped crystals have been demonstrated with the development of the crystal design and growth and the innovations of the laser technology. Figure 2(b) shows the room temperature CW output power and the corresponding slope efficiency obtained with $Er^{3+}$ ions-doped crystalline lasers in the 2.7–3 μm region. In 1992, Dinerman *et al.* reported the first, to the best of our knowledge, CW operation of monolithic Er:YAG, Er:GGG, and Er:YSGG lasers near 3 μm with output powers of 143, 155, and 190 mW[61], which were further promoted to 171, 293, and 511 mW in 1994[46]. In 2010, Sousa *et al.* realized a maximum CW output power of 1.5 W with an Er:YAG crystal at 2.94 μm[82]. In 2014, You reported a diode-end-pumped MIR multi-wavelength Er,Pr:GGG laser with CW output power of 324 mW[57]. In 2015, Shen *et al.* studied the CW laser performance of an LD side-pumped Er:YSGG slab at 2.79 μm, in which the maximum output power of 1.84 W was obtained with a slope efficiency of 10.2%[83]. The corresponding experiment setup is shown in Fig. 2(c), in which an Er:YSGG slab with dimensions of 1 mm × 2 mm × 12 mm was dual-side-pumped by 970 nm LDs. In 2018, Yu *et al.* realized a high-efficiency Er:YGG laser at 2.82–2.92 μm with output power of 1.38 W and slope efficiency of 35.4%, approaching the theoretical quantum limits[84]. For fluoride crystals, in 2006, Basiev presented a continuously tunable CW laser operation near 2.75 μm of diode-pumped Er:$SrF_2$ and Er:$CaF_2$ crystals with output powers of 0.4 and 2 W[70]. In 2018, Švejkar *et al.* promoted the Er:$SrF_2$ laser output power up to 1.3 W with a slope efficiency of 9.2% and tuning range of 123 nm[72]. Liu *et al.* realized an efficient CW laser performance of a diode-end-pumped Er:$CaF_2$-$SrF_2$ crystal with an output power of 712 mW and a slope efficiency of 41.4%[71]. However, as shown in Fig. 2(b), the output powers of the garnet structure and fluoride-crystals-based $Er^{3+}$-doped crystal lasers

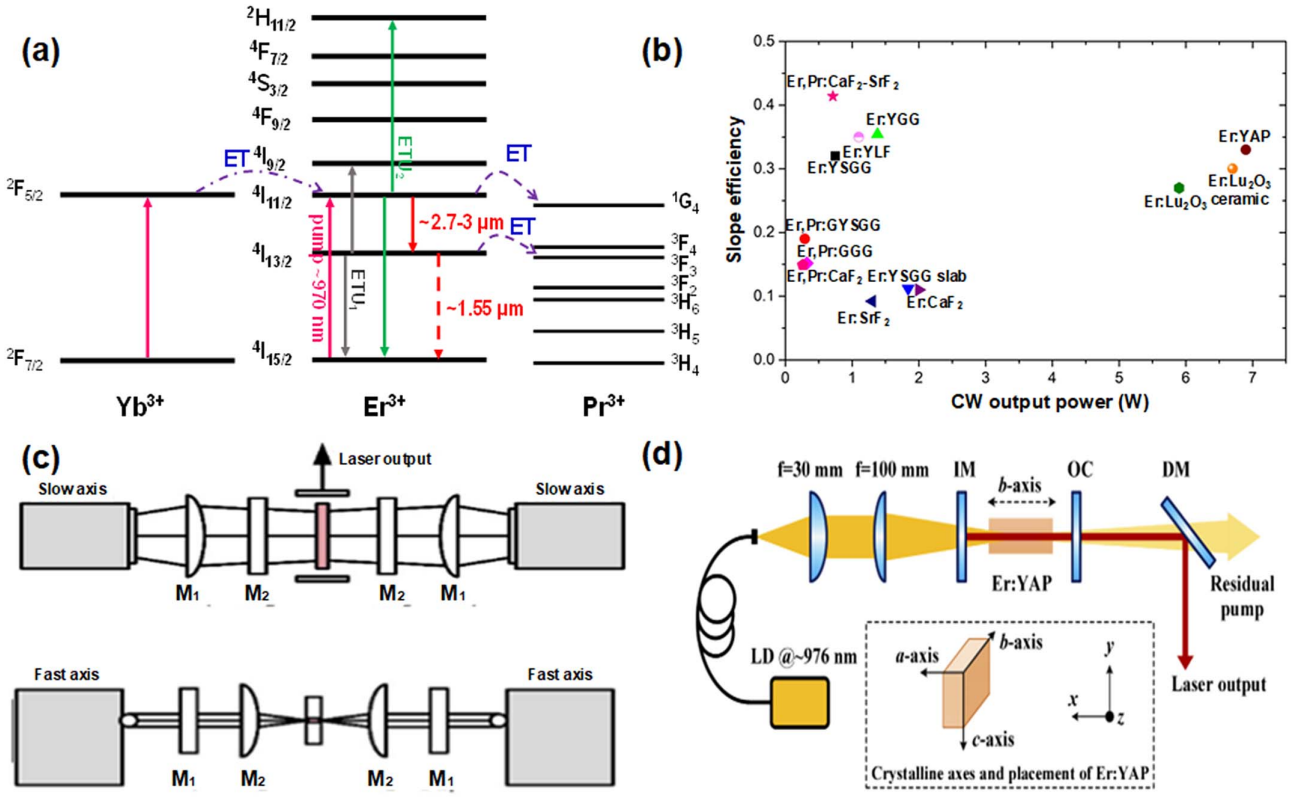


**Fig. 2.** (a) Simplified energy-level diagram of $Er^{3+}$-doped gain medium and sensitizer and deactivated effect of $Yb^{3+}$ and $Pr^{3+}$ ions; (b) the summary of the room temperature CW output power and slope efficiency of Er-doped crystalline lasers at 2.7–3 μm; (c) the schematic of a diode-side-pumped Er:YSGG slab laser at 2.79 μm[83]; (d) the experimental setup of the LD end-pumped high-power Er:YAP laser[15].

**Table 1.** Laser Performance of CW Er-Doped Solid-State Crystal Lasers.

| Gain Medium | $Er^{3+}$-Doping Concentration (at.%) | Output Power (W) | Slope Efficiency (%) | Emission Wavelength (μm) | Ref. |
|---|---|---|---|---|---|
| Er:YAG crystal | 50 | 1.5 | – | 2.94 | [82] |
| Er:GGG crystal | 30 | 0.29 | 19 | 2.8 | [46] |
| Er:YSGG crystal | 30 | 0.75 | 32 | 2.8 | [67] |
| Er:YGG crystal | 10 | 1.38 | 35.4 | 2.82–2.92 | [84] |
| Er:YSGG slab crystal | 38 | 1.84 | 11.2 | 2.79 | [83] |
| Er,Pr:GGG | 30 | 0.324 | 15.18 | 2.8 | [57] |
| Er,Pr:GYSGG | 20 | 0.284 | 17.4 | 2.79 | [90] |
| Er:YLF crystal | 15 | 1.10 | 35 | 2.8 | [91] |
| Er:$CaF_2$ crystal | 5 | 2 | 11 | 2.75 | [70] |
| Er:$SrF_2$ crystal | 3 | 1.3 | 9.2 | 2.75 | [72] |
| Er,Pr:$CaF_2$ crystal | 3 | 0.262 | 14.9 | 2.803 | [58] |
| Er,Pr:$CaF_2$-$SrF_2$ crystal | 4 | 0.712 | 41.4 | 2.73 | [71] |
| Er:$Lu_2O_3$ crystal | 7 | 5.90 | 27 | 2.9 | [49] |
| Er:$Y_2O_3$ ceramic | 2 | 14.00 | 26 | 2.7 | [87] |
| Er:$Y_2O_3$ ceramic | 0.25 | 24 | 14 | 2.74 | [86] |
| $Er^{3+}$:$Lu_2O_3$ ceramic | 11 | 6.70 | 30 | 2.8 | [88] |
| Er:YAP crystal | 5 | 6.90 | 33 | 2.9 | [15] |

in the 2.7–3 μm region are limited to ~2 W, mainly because of the severe thermal effect. Benefiting from the high thermal conductivity and low phonon energy, sesquioxide crystals have been proved to be more suitable for high-power MIR laser operation. In 2012, Li *et al.* presented a 5.9 W CW output power with Er:$Lu_2O_3$ as the gain medium and a slope efficiency of 27%[49]. Besides sesquioxide crystals, high-quality polycrystalline transparent sesquioxide ceramics also show huge opportunities for high-power 3 μm lasers because of the advantages compared to single crystals, such as excellent mechanical strength and easy fabrication process[76,77,79,85–87]. In 2011, a 2.8 μm Er:$Y_2O_3$ ceramic laser with an output power of 14 W was reported with a cooling temperature of 77 K[87], which was promoted to be 24 W in 2016[86]. Very recently, Yao *et al.* demonstrated an Er:$Lu_2O_3$ ceramic laser at 2845 nm with 6.7 W output power and > 30% slope efficiency, which is the highest output power ever achieved from Er-doped sesquioxide ceramics at room temperature[88]. Besides, YAP is another attractive host candidate for high-power $Er^{3+}$-doped crystal lasers owing to low phonon energy and excellent thermal properties. In 2019, Yasuhara *et al.* presented a 1.17 W CW Er:YAP crystal laser operating at 2.9 μm with a slope efficiency of 29%[89]. Subsequently, due to the anisotropic thermal properties, a *b*-cut Er:YAP crystal was chosen, and the output power was promoted to 6.9 W [as shown in Fig. 2(d)], which is the highest CW output power generated from Er-doped solid-state lasers at room temperature[15]. Table 1 summarizes the important results of CW Er-doped solid-state lasers.

In the pulsed regime, flash-side pumping is an effective and commonly used architecture to produce high-energy 2.7–3 μm laser pulses at low repetition rate. As early as 1990, pulse energy as high as 400 mJ was obtained with an Er:YAG crystal under the pump energy of 92 J[92]. However, the pulse width was always in the scale of hundreds of microseconds or even milliseconds without any cavity *Q*-factor modulation. Combining with the active or passive *Q*-switching technique, nanosecond 2.7–3 μm pulsed lasers could be achieved. In 2004, a pulse energy of 137 mJ with a pulse width of ~90 ns and repetition rate of 3 Hz was obtained from a single xenon flashlamp-pumped, actively *Q*-switched Er:YAG laser at 2.94 μm[93]. In 2005, Koranda *et al.* reported a 60 ns laser pulse with energy of 60 mJ generated to form a $LiNbO_3$ (LN) electro-optically (EO) *Q*-switched 2.94 μm Er:YAG laser[94], as shown in Fig. 3(a). An Er:YAG crystal with dimensions of Φ4 mm (diameter) × 89 mm (length) was placed along the Xe flashlamp in a Linear Matrix Inequality diffuse ceramic cavity, which was the key part of the laser oscillator. The LN crystal with both faces cut under a Brewster angle acted as a Pockels cell and optical polarizers. The specially designed delay circuit was another key element to provide precise switching of the EO shutter at the time when the population inversion inside the Er:YAG crystal reached the maximum value. In 2007, a giant pulse width of 35 ns and an output energy up to 30 mJ were obtained from a $Fe^{2+}$:ZnSe passively *Q*-switched Er:YAG laser at 2.94 μm[95]. In 2013, Wang *et al.* realized a 2.79 μm high-peak-power langasite (LGS) EO *Q*-switched Cr,Er:YSGG laser with pulse energy of 216 mJ and pulse duration of 14.36 ns[96]. For the flash-pumping laser system, it is difficult to achieve high pulse energy at a high repetition rate due to the low operation repetition rate, low conversion efficiency, and strong thermal effect.

Compared to flash pumping, pulsed LD pumping has the merits of high efficiency, better beam quality, and high repetition rate. Hence, an efficient and compact diode-laser-pumped 2.94 μm Er:YAG laser with energy up to 9 mJ was realized in 2010, consequently making the hermetically sealed windowed package[82]. In 2015, a pulse energy of 562 mJ at 16 Hz was obtained from an LD side-pumped 2.79 μm Er:YSGG laser[97]. In 2017, an output peak power of 1.2 W was obtained by a quasi-CW LD end-pumped Er:$Lu_2O_3$ laser[77]. In 2018, a maximum output power of 8.86 W was achieved at 125 Hz with a slope efficiency of 14.8% from an LD-side-pumped Er,Pr:$Gd_{1.17}YSc_{1.284}Ga_3O_{12}$ laser[60]. As shown in Fig. 3(b), the main part was the diode-side-pumped Er,Pr:GYSGG module, in which three LD arrays were symmetrically placed with intervals

of 120° to alleviate the thermal effect. For CW LD pumping, pulsed Er-doped laser generation at 2.7–3 μm is mainly focused on the passive *Q*-switching technique. The typical traditional saturable absorber (SA), semiconductor SA mirror (SESAM), and Fe:ZnSe have been applied in Er-doped crystal laser resonators to generate nanosecond pulsed lasers at 2.7–3 μm. In 2018, Qin *et al.* realized a passively *Q*-switched Er:$Y_2O_3$ ceramic laser by using SESAM as the SA, generating a pulse energy of 1.7 μJ and a pulse duration of 350 ns at 2709.3 nm[98]. In 2019, Zhang *et al.* reported a sub-15-ns passively *Q*-switched Er:YSGG laser at 2.8 μm with Fe:ZnSe as the SA, in which a pulse energy of 5.05 μJ and a pulse width of 14.6 ns were obtained[99]. The schematic of the experimental setup and the passive *Q*-switching output characters are shown in Figs. 3(c) and 3(d). The Fe:ZnSe crystals with a doping concentration of 0.18% and thickness of 0.6 and 0.8 mm (corresponding to the initial transmissions of 55.4% and 50.2%) were used as the SAs. In order to get the short pulse width, the output coupler was directly attached to the rear surface of the Fe:ZnSe crystal to form the "microchip" structure and compress the cavity length to be approximately equal to the length of the laser crystal and SA (~5.6 and 5.8 mm). Nevertheless, SESAM and Fe:ZnSe suffer several drawbacks, including complex and costly fabrication process, narrow saturable absorption band, and slow recovery time, which significantly limit their applications. Since the first, to the best of our knowledge, demonstration of a graphene SA in 2009[100], studies on 2D materials-based SAs have experienced a boom in development due to the advantages of fast relaxation time, proper modulation depth and saturation intensity, broad operation wavelength band, and easy fabrication. In 2017, the passively *Q*-switched Er:YSGG lasers at ~2.8 μm were demonstrated by utilizing the composite $Bi_2Te_3$/graphene and $ReS_2$ as SAs, generating the pulse width of 243 and 324 ns, respectively[101,102]. By using bismuth nanosheets (Bi-NSs), MXene $Ti_3C_2T_x$, and black phosphorus (BP), Liu *et al.* realized *Q*-switched $Er^{3+}$-doped lasers with pulse widths of 980, 814, and 702 ns, respectively[103–105]. Besides, as the typical materials of transition metal dichalcogenides (TMDs), $MoS_2$, $WS_2$, $ReSe_2$, and $TiSe_2$ were also applied in MIR passively *Q*-switched lasers to generate the shortest pulse durations of 335, 679, 202, and 160 ns, respectively[106–109]. The performances of diode-end-pumped passively *Q*-switched Er-doped crystalline lasers are summarized in Table 2.

Besides the *Q*-switched pulsed lasers, the mode-locked Er-doped ultrafast lasers are of great interest for some practical applications, owing to the ultrashort pulse width and high peak

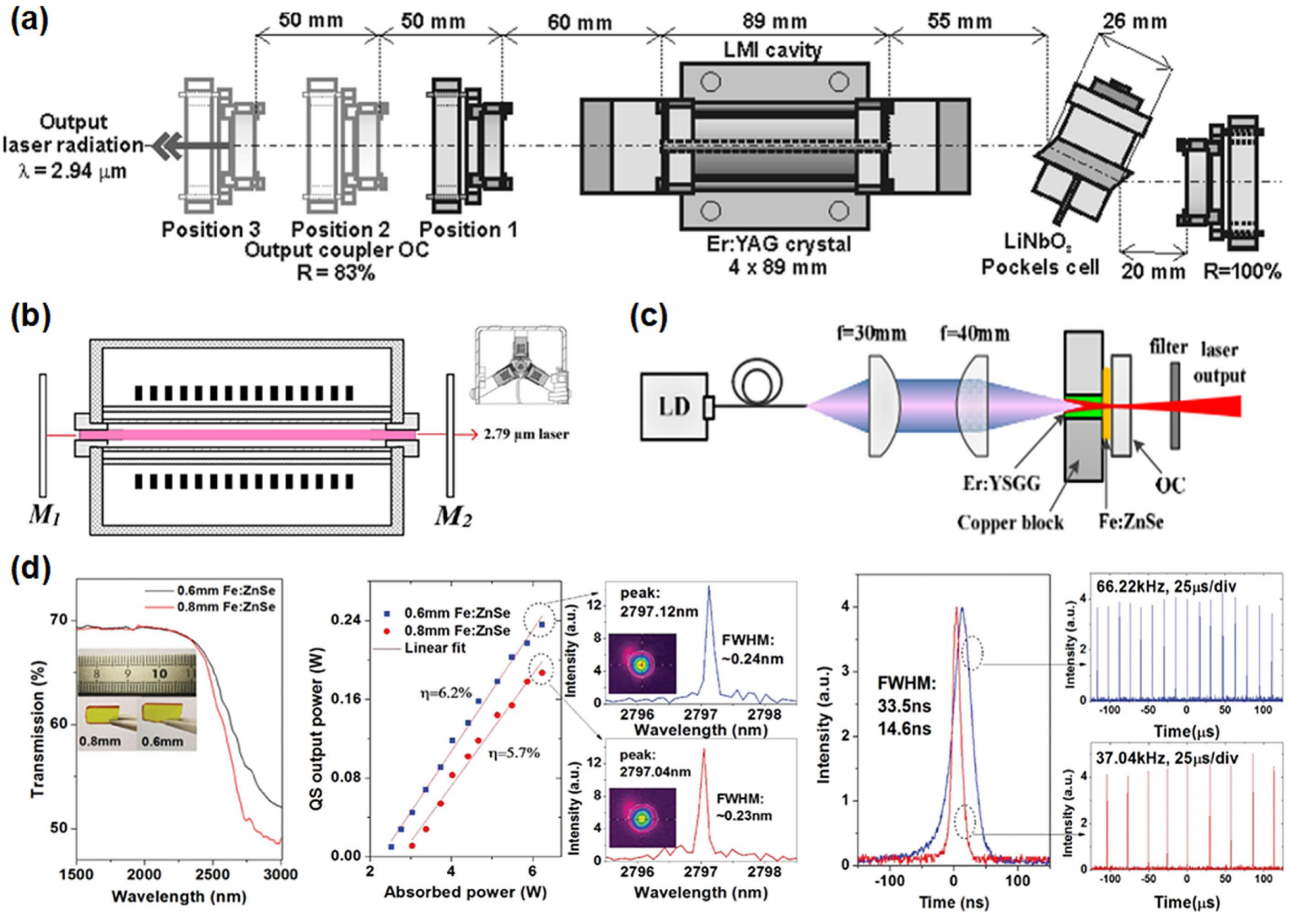


**Fig. 3.** (a) Experimental setup of high-energy LN EO *Q*-switched Er:YAG laser[94]; (b) the schematic diagram of the LD arrays side-pumped Er,Pr:GYSGG laser (inset: side-pumped symmetry)[60]; (c) the experimental setup and (d) output characterizations of the Fe:ZnSe passively *Q*-switched Er:YSGG laser[99].

**Table 2.** Laser Performance of Diode-End-Pumped Passively *Q*-Switched $Er^{3+}$-Doped Crystalline Lasers.

| Gain Medium | SA | Output Power (mW) | Slope Efficiency (%) | Pulse Width (ns) | Pulse Repetition Rate (kHz) | Peak Power (W) | Pulse Energy (μJ) | Ref. |
|---|---|---|---|---|---|---|---|---|
| Er:$Y_2O_3$ ceramic | SESAM | 223 | 13.5 | 350 | 130.6 | 4.9 | 1.71 | [98] |
| Er:YSGG crystal | Fe:ZnSe | 187 | 5.7 | 14.6 | 37.04 | 345.8 | 5.05 | [99] |
| Er:YSGG crystal | $Bi_2Te_3$/G | 110 | – | 243 | 88 | 5.14 | 1.25 | [101] |
| Er:YSGG crystal | $ReS_2$ | 104 | 27.3 | 324 | 126 | 2.56 | – | [102] |
| Er:$SrF_2$ crystal | Bi-NSs | 226 | 13.6 | 980 | 56.20 | 4.10 | 4.02 | [103] |
| Er:$CaSrF_2$ crystal | $Ti_3C_2T_x$ | 286 | 14.0 | 814 | 45.5 | 7.76 | 6.32 | [104] |
| Er:$SrF_2$ crystal | BP | 180 | 7.9 | 702 | 77.03 | 2.34 | 3.3 | [105] |
| Er:$Lu_2O_3$ crystal | $MoS_2$ | 1030 | 17.1 | 335 | 121 | 8.5 | 23.8 | [106] |
| Er:$SrF_2$ crystal | $WS_2$ | 428 | 18.2 | 679 | 38 | 11.26 | 16.58 | [107] |
| Er:YAP crystal | $ReSe_2$ | 526 | 14.8 | 202.8 | 244.6 | 2.2 | 10.6 | [108] |
| Er:YSGG crystal | $TiSe_2$ | 250 | – | 160 | 78 | 13.92 | – | [109] |
| Er:$Y_2O_3$ crystal | Graphene | 115 | – | 296 | 44.2 | 2.59 | 8.77 | [110] |

power. Picosecond or even femtosecond CW mode-locked Er-doped fiber lasers have been extensively studied and realized[111–116], while only *Q*-switched mode-locked operation was obtained for Er-doped crystalline lasers because the intracavity pulse energy could not be high enough to reach the stable CW mode-locking regime caused by the relatively low gain and absorption of $H_2O$. In 2018, Xue *et al.* realized a stable *Q*-switched mode-locked 2.7 μm Er:$Y_2O_3$ ceramic laser with SESAM, generating an average output power of ~92 mW with 100% modulation depth and 130 MHz repetition rate embedded in the *Q*-switched envelope of ~1.2 μs width[85]. Liu *et al.* reported passively *Q*-switched mode-locked Er:$CaF_2$-$SrF_2$ lasers with the repetition rate of 136.3 MHz inside the *Q*-switched envelope and a pulse width estimated to be 1.78 ns[71].

## 2.2 $Ho^{3+}$-doped crystalline lasers in the 2.7–3 μm region

The $Ho^{3+}$ ion is another promising candidate for generating 2.7–3 μm lasers related to the $^5I_6 \rightarrow {}^5I_7$ transition, as shown in Fig. 4(a). However, Ho-doped crystalline lasers emitting in the 2.7–3 μm spectral region are much less studied compared to those emitting around ~2.1 μm and $Er^{3+}$-doped lasers. The main limiting issues are the pumping wavelength around ~1150 nm (not the commercial emitting wavelength of a LD) and the same self-terminated effect occurring with the $Ho^{3+}$:$^5I_6 \rightarrow {}^5I_7$ transition ($Ho^{3+}$:$^5I_7$ has a longer lifetime than $Ho^{3+}$:$^5I_6$, resulting in the lower laser level during oscillation). The same as the $Er^{3+}$:$^4I_{11/2} \rightarrow {}^4I_{13/2}$ transition, the saturation of the $Ho^{3+}$:$^5I_6 \rightarrow {}^5I_7$ transition can also be suppressed by cascade lasing ($Ho^{3+}$:$^5I_6 \rightarrow {}^5I_7$ and $Ho^{3+}$:$^5I_7 \rightarrow {}^5I_8$ transitions) or co-doping with sensitized (typically $Yb^{3+}$ ions) or deactivated ions (typically $Nd^{3+}$ and $Pr^{3+}$ ions)[5,9,39,117–125]. The host materials are also focused on the garnet structure and fluoride.

In the beginning, Ho-doped crystalline lasers operating in the 2.7–3 μm spectral region were mainly pumped by a flashlamp or pulsed laser due to lack of pumping source and the population bottleneck effect. In 1987, Machan *et al.* realized the simultaneous lasing of $Nd^{3+}$ and $Ho^{3+}$ ions at 1.064, 1.339, 2.94, and 3.011 μm with a flashlamp-pumped Ho:Nd:YAG crystal, indicating that the strong ion-ion interaction could produce efficient 3 μm lasing[117].

In 1990, Anthon reported the first laser (Q-switched Nd:YAG laser operating at 1123 nm) pumped 3 μm Ho:YAG and Ho:GGG laser[126]. In 1996, Umyskov *et al.* demonstrated a flashlamp-pumped $Cr^{3+}$:$Yb^{3+}$:$Ho^{3+}$:YSGG laser with the emission wavelength continuously tuned from 2.84 to 3.05 μm, in which co-doping with $Cr^{3+}$ and $Yb^{3+}$ ions could efficiently increase the absorption of the pump light by the energy transfer of $Cr^{3+} \rightarrow Yb^{3+} \rightarrow Ho^{3+}$[118,127]. In 2002, Lukashev demonstrated a flashlamp-pumped Cr,Yb,Ho:YSGG laser at 3 μm with an output energy of 62 mJ[128].

In 1998, Diening *et al.* realized 11 and 2.5 mW CW laser output at 2.84 μm with an $Yb^{3+}$:$Ho^{3+}$:$KYF_4$ crystal pumped by a Ti:$Al_2O_3$ laser and LD, respectively[129]. In 2000, they reported another lasing of an Yb,Ho:YAG crystal around 1.2 and 3 μm, in which the quasi-CW laser emission at 2844 nm with pulse energy up to 10.5 mJ was obtained[119]. In 2017, our group realized a 1150 nm LD end-pumped Ho,Pr:LLF laser with CW output power of 172 mW and a slope efficiency of 10.8%[9]. Then, by using a high-power and high-beam-quality 1150 nm Raman

laser as the pump source, the CW output power was promoted to 1.15 W with a slope efficiency of 15.5%[130]. In 2019, by optimizing the doping concentration of $Ho^{3+}$ and $Pr^{3+}$ ions in the Ho, Pr:YLF crystal, the lifetime of $Ho^{3+}$:$^5I_6$ was designed to be larger than that of $Ho^{3+}$:$^5I_7$, as shown in Fig. 3(b). Thus, as high as 1.27 W CW laser output with a slope efficiency of 28.3% was obtained[131], as shown in Fig. 4(c). By using the dual-end-pumping configuration, a maximum output power of 1.46 W was obtained with a slope efficiency of 7.7%. To the best of our knowledge, it is the largest CW output power ever obtained with Ho-doped crystalline lasers[132]. Table 3 summarizes the flashlamp-pumped and CW laser performance of Ho-doped MIR lasers in the 2.7–3 μm region.

In the pulsed regime, besides the microsecond pulse generated by pumping with the flashlamp and pulsed LD, nanosecond pulses were obtained with the active and passive *Q*-switching techniques. For passive *Q*-switching operation, SAs are mainly focused on low-dimensional materials. In 2017, our group realized a 2.95 μm diode-end-pumped passively *Q*-switched Ho,Pr:LLF laser with graphene as an SA, generating a maximum average output power of 88 mW with pulse width of 937.5 ns and repetition rate of 55.7 kHz[9]. Then, by using BP as the SA and a Raman fiber laser as the pump source, a pulse width of 194.3 ns with a repetition rate of 158.7 kHz and average output power of 385 mW was obtained[135]. With other low-dimensional materials as SAs, such as 2D TMDs ($MoSe_2$, $TiSe_2$, etc.), graphitic carbon nitride (g-CN), and gold nanospheres, passively *Q*-switched laser operation with the pulse widths of 731.5, 160.5, 420, and 743 ns was obtained[136–139]. With the SESAM as the SA, Liu realized a passively *Q*-switched Ho,Pr:LLF laser at 2.9 μm with a pulse duration of 395 ns and repetition rate of 7.29 kHz[140]. For active *Q*-switching operation, a high-repetition-rate (compared to flashlamp pumping) kilohertz (kHz) actively *Q*-switched Ho,Pr:YLF laser at 2.9 μm was realized with LN as the electro-optical *Q* switch, in which the shortest pulse width of 25.2 ns was obtained with the repetition rate of 500 Hz and single pulse energy of 0.4 mJ[132].

The corresponding schematic experimental setup and the relationship between the output power and incident pump power are shown in Figs. 4(d) and 4(e). Table 4 summarizes the actively and passively *Q*-switched laser performance of Ho-doped crystalline lasers in the 2.7–3 μm region.

## 2.3. $Dy^{3+}$-doped all solid-state crystalline lasers in the 2.7–3 μm spectral region

The $Dy^{3+}$ ion is also a most promising and efficient candidate for emitting MIR laser wavelengths around ~3 μm based on its energy-level structure with the $Dy^{3+}$:$^6H_{13/2} \rightarrow {}^2H_{15/2}$ transition. The study of Dy-doped MIR lasers is much less than that of $Er^{3+}$ and $Ho^{3+}$ ions, basically because of the lack of high-quality crystals and pump sources. Figure 5(a) shows the simplified energy-level diagram of the $Dy^{3+}$ ion. The absorption bands of the $Dy^{3+}$ ion are located in the near-infrared region (around 1.1, 1.3, and 1.7 μm). Same as the $Er^{3+}$ and $Ho^{3+}$ ions, the possibility of realizing laser emission from the

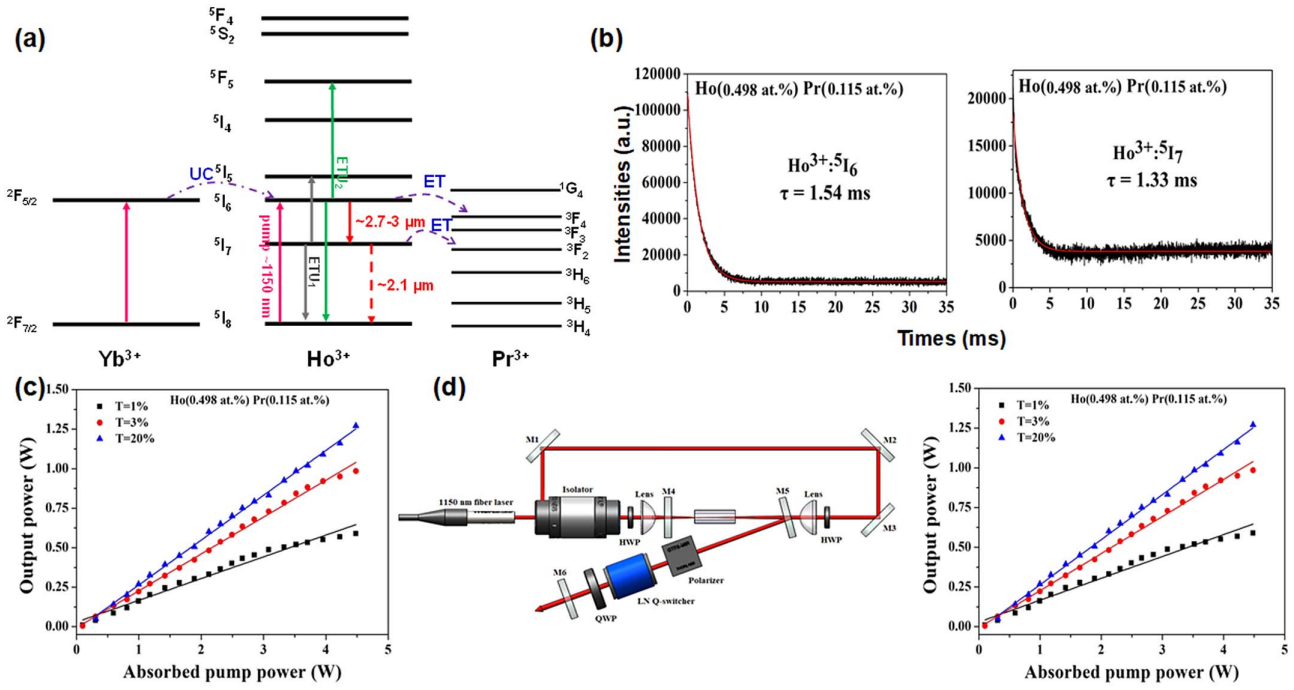


**Fig. 4.** (a) Simplified energy-level diagram of $Ho^{3+}$-doped gain medium and sensitizer and deactivated effect of $Yb^{3+}$ and $Pr^{3+}$ ions; (b) the fluorescence life time "reversion" of Ho:$^5I_6$ and Ho:$^5I_7$ in Ho,Pr:YLF crystals with doping concentrations of 0.498 at.% and 0.115 at.% for $Ho^{3+}$ and $Pr^{3+}$ ions[131]; (c) the output laser power of a Raman laser end-pumped Ho,Pr:YLF ($Ho^{3+}$: 0.498 at.% and $Pr^{3+}$: 0.115 at.%) laser[131]; (d) the experimental setup and laser output power of dual-end-pumped EO *Q*-switched Ho,Pr:YLF laser[132].

**Table 3.** Flashlamp-Pumped and CW Laser Performance of Ho-Doped 2.7–3 μm MIR Lasers.

| Pump Source | Gain Medium | $Ho^{3+}$ Doping Concentration (at.%) | Output Power/Energy | Slope Efficiency (%) | Emission Wavelength (μm) | Ref. |
|---|---|---|---|---|---|---|
| Flashlamp | Ho,Nd:YAG | 10 | 41 mJ at 2.94 and 3.011 | 0.012 at 2.94 and 3.011 μm | 1.064, 1.339, 2.94, and 3.011 | [117] |
| 1123 nm *Q*-switched Nd:YAG laser | Ho:YAG | 30 | – | 6 | 2.94 | [126] |
| Flashlamp | Ho:$YAlO_3$ | 2 | 42 mJ | 0.05 | 3.019 | [133] |
| 1.08 μm NdYAlO laser | Ho:$YAlO_3$ | 2 | – | 1 at 2.92 | 2.844–3.017 | [134] |
| Flashlamp | Cr,Yb,Ho:YSGG | – | ~520 mJ | ~0.35 | 2.84–3.05 | [127] |
| Ti:$Al_2O_3$ laser and 970 nm LD | Yb,Ho:$KYF_4$ | 0.5 | 11.5 and 2.5 mW | 1 and 0.3 | 2.84 | [129] |
| 970 nm LD | Yb,Ho:YSGG | 1 | 10.5 mJ | 3.9 | 2.9 | [119] |
| 1150 nm LD | Ho,Pr:LLF | 0.185 | 0.172 mW | 10.8 | 2.95 | [9] |
| 1150 nm Raman fiber laser | Ho,Pr:LLF | 0.185 | 1.15 W | 15.5 | 2.95 | [130] |
| 1150 nm fiber laser | Ho,Pr:YLF | 0.498 | 1.27 W | 28.3 | 2.9 | [131] |
| 1150 nm Raman fiber laser | Ho,Pr:YLF | 0.498 | 1.46 W | 7.7 | 2.95 | [132] |

**Table 4.** Actively and Passively *Q*-Switched Laser Performance of 2.7–3 μm Ho-Doped Crystalline Lasers.

| Gain Medium | *Q* Switch | Output Power (mW) | Pulse Width (ns) | Pulse Repetition Rate (kHz) | Peak Power (W) | Pulse Energy (μJ) | Ref. |
|---|---|---|---|---|---|---|---|
| Ho,Pr:LLF | g-CN | 101 | 420 | 93 | 2.86 | 1.1 | [138] |
| Ho,Pr:LLF | BP | 385 | 194.3 | 158.7 | 12.5 | 2.4 | [130] |
| Ho,Pr:LLF | Monolayer graphene | 88 | 937.5 | 55.7 | 1.4 | 1.6 | [9] |
| Ho,Pr:LLF | $MoSe_2$ | 58 | 818.8 | 71.05 | 1.12 | 0.82 | [136] |
| Ho,Pr:LLF | Au-NPs | 268 | 734 | 91 | 4.02 | 2.95 | [139] |
| Ho,Pr:YLF | EO *Q* switch | 268 | 25.2 | 0.5 | 15,900 | 400 | [132] |
| Ho,Pr:LLF | 1 T-$TiSe_2$ | 130 | 160.5 | 98.8 | 8.2 | 1.32 | [137] |
| Ho,Pr:LLF | SESAM | 160 | 395 | 7.29 | 51.1 | 20.2 | [140] |

$Dy^{3+}$:$^6H_{13/2} \rightarrow {}^2H_{15/2}$ transition around ~3 μm depends on the host crystal material choice, which should possess low photon energy and weak ion to crystal lattice orbital coupling and therefore can efficiently decrease corresponding non-radiative losses and increase the quantum efficiency. To date, the $Dy^{3+}$:$^6H_{13/2} \rightarrow {}^2H_{15/2}$ transition has been obtained in fluoride crystals, such as Dy:$BaYb_2F_8$ and Dy:$BaY_2F_8$. In 1973, Johnson *et al.* demonstrated a flashlamp-pumped Dy:$BaY_2F_8$ laser operating at 3.022 μm[141]. In 1982, a $Dy^{3+}$:$BaYb_2F_8$ MIR laser at 3.02 μm pumped by a 1.06 μm Nd:YAG laser was demonstrated[142]. In 1997, Djeu *et al.* realized a room temperature $Dy^{3+}$:$BaYb_2F_8$ laser at 3.4 μm pumped by a pulsed 1.3 μm Nd:YAG laser[142]. Unfortunately, there are no reports about CW $Dy^{3+}$-doped crystalline lasers. But, for the fiber laser, Jackson has realized room temperature 2.9 μm CW laser emission with output power of 0.275 W and slope efficiency of 4.5% from a 1100 nm fiber-laser-pumped Dy:ZBLAN fiber in 2003[18]. In 2006, they realized a CW Dy:ZBLAN fiber laser with a maximum output power of 180 mW and a slope efficiency of 20%, in which the pump source was an ~1.3 μm Nd:YAG laser[143]. In 2016, they reported a high-efficiency 3.04 μm Dy:ZBLAN fiber laser with a record slope efficiency of 51% pumped by a 2.8 μm Er:ZBLAN laser[144]. Moreover, they also realized the acousto-optically and passively *Q*-switched Dy:ZBLAN fiber laser with the central wavelength tunable from 2.97 to 3.23 μm[145]. The actively *Q*-switched Dy:ZBLAN fiber

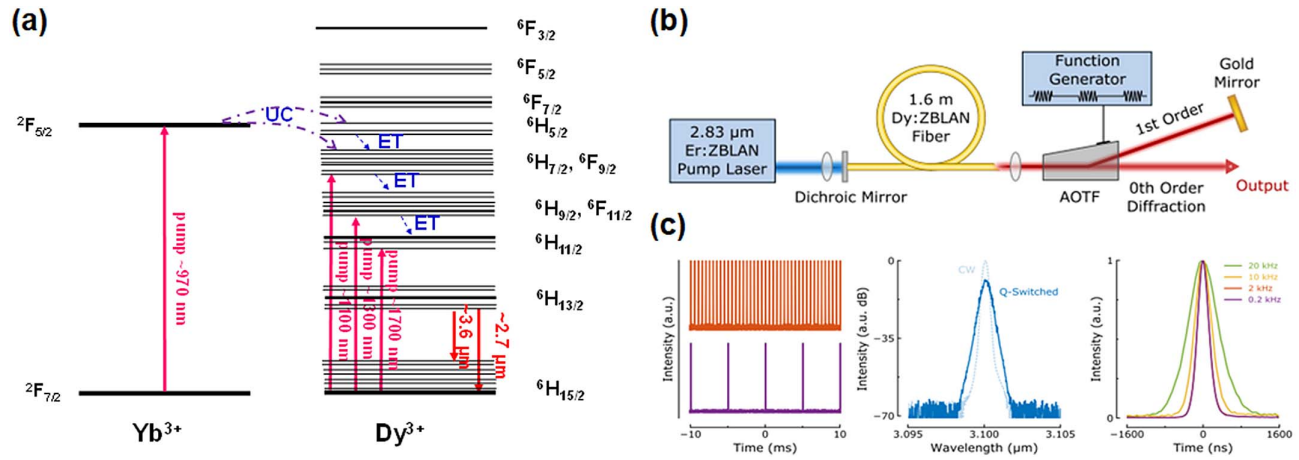


**Fig. 5.** (a) Simplified energy-level diagram of $Dy^{3+}$-doped gain medium and sensitizer effect of $Yb^{3+}$ ions; (b) and (c) are the schematic of the actively *Q*-switched Dy:ZBLAN fiber laser and corresponding laser output characterizations[145].

laser schematic is shown in Fig. 5(b), where the acousto-optic tunable filter (AOTF) comprises an anisotropic $TeO_2$ crystal in "slow shear operation." The corresponding actively *Q*-switched laser characterization with 450 mW pump power is shown in Fig. 5(c). In 2019, Luo *et al.* realized a gain-switched $Dy^{3+}$-doped ZBLAN fiber laser around 3 μm by using an actively *Q*-switched $Yb^{3+}$-doped fiber laser at 1.1 μm as the pump source, yielding a repetition rate of 80 kHz and a pulse width of 300 ns[146].

However, it is a real drawback for establishing a compact MIR laser because of the pumping wavelength not corresponding to any commercially available high-power LDs. Therefore, researchers try to study the sensitized ions that can transfer pumping energy to the $Dy^{3+}$ ion to allow optical pumping with commercially available LDs. $Yb^{3+}$ ions have been proved to be the most efficient sensitized ions for $Dy^{3+}$ ions-doped 3 μm MIR laser emission with energy transformation from $Yb^{3+}$:$^2F_{5/2}$ to $Dy^{3+}$:$^6H_{5/2}$, which enables it to be pumped by the commercial 970 nm LD[147,148]. The simplified energy-level diagram of $Yb^{3+}$, $Dy^{3+}$ co-doped crystals is shown in Fig. 5(b). In 2015, Zhang et.al presented the successful growth of a $Yb^{3+}$, $Dy^{3+}$:$PbF_2$ crystal, in which the energy-transfer efficiency from $Yb^{3+}$ to $Dy^{3+}$ was as high as (97.7 ± 0.3)%. In addition, this crystal possesses long fluorescence lifetime of 15.4 ms and high quantum efficiency of 95%[148].

## 3. Challenges and Outlook

Expanding the laser wavelength to the MIR region is one of the most important developing trends of laser technology. To date, laser sources with directly emitting wavelengths at 2.7–3 μm are mainly based on $Er^{3+}$, $Ho^{3+}$, and $Dy^{3+}$ rare-earth ions-doped gain media, in which $Er^{3+}$ ions are mostly studied, $Ho^{3+}$ ions take second place, and $Dy^{3+}$ ions are the least studied. Compared to the rare-earth-doped fiber lasers, the rare-earth-doped crystalline lasers experience a relatively slow development mainly because of the lack of high-quality laser crystals. But, the solid-state crystalline lasers are compact and efficient all solid-state coherent laser sources with the merits of low undesirable nonlinear effects and large mode area and therefore have great advantages in producing high-energy and high-peak-power ultrafast lasers. In this review, we mainly summarize the state-of-the-art developments of all solid-state MIR crystalline lasers in the 2.7–3 μm spectral region based on $Er^{3+}$, $Ho^{3+}$, and $Dy^{3+}$-doped crystals. However, there are still several challenges, and a series of potential studies need to be further pursued in the future.

First, the host material selection and the preparation of the high-quality crystals are the basis for high-power and high-efficiency solid-state MIR crystalline lasers in the 2.7–3 μm region. The longer the emitting wavelength, the narrower the bandgap between the upper and lower laser level, which, thus, results in the larger non-radiative transition loss. Therefore, for MIR laser emission, the host material should have low phonon energy to reduce the probability of non-radiative transitions. In addition, the host materials should have large thermal conductivity to mitigate the relatively heavy thermal effect of the MIR crystalline lasers. The damage threshold is another important issue for high-power and high-energy laser operation.

Second, the selection of sensitized and deactivated ions and the doping concentration are also important for rare-earth-doped crystalline lasers at 2.7–3 μm. For $Er^{3+}$ and $Ho^{3+}$ ions-doped crystals, the deactivated ions are important for solving the "self-terminated" bottleneck to realize the high-efficiency laser operation. For $Ho^{3+}$ and $Dy^{3+}$ ions-doped crystals, the sensitized ions are important for selecting the commercial LD as the pump source. Besides, the doping concentrations of both excited and sensitized or deactivated ions should be further optimized.

Third, cascade laser operation is very attractive for multi-wavelength MIR laser generation. Based on the energy-level diagram of $Er^{3+}$, $Ho^{3+}$, and $Dy^{3+}$ ions, the cascade laser operation not only provides a multi-wavelength MIR laser source, but also

enhances the 2.7–3 μm laser generation. The cascade laser operation of $Er^{3+}$ and $Ho^{3+}$ ions-doped fiber lasers has been realized, while it still remains a big challenge for crystalline lasers.

Fourth, mode-locked laser operation is another challenge for rare-earth-doped crystalline lasers at 2.7–3 μm. The mode-locked laser operation in the near-infrared (1.0, 1.3, 1.5 μm) and MIR (2.0, 2.4 μm) regions has been widely studied, and picosecond or even femtosecond pulses have been generated. Due to the lack of suitable SAs and the absorption of $H_2O$, it is very difficult to achieve the mode-locking operation of rare-earth-doped crystalline lasers at 2.7–3 μm. However, with the innovations of ultrafast laser technology and material science, it is something to look forward to and can be widely applied in the fields of strong field physics, optical frequency comb, ultrafast spectroscopy and microimaging, etc.

## Acknowledgement

This work was supported by the National Natural Science Foundation of China (Nos. 61975095, 61975097, and 61308042), the Young Scholars Program of Shandong University (No. 2017WLJH48), the Youth Cross Innovation Group of Shandong University (No. 2020QNQT), and the Financial Support from Qilu Young Scholar of Shandong University.

## References

1. H. Gebbie, W. Harding, C. Hilsum, A. Pryce, and P. Sciences, "Atmospheric transmission in the 1 to 14 μm region," Proc. R. Soc. A **206**, 87 (1951).
2. L. S. Rothman, R. Gamache, R. Tipping, C. Rinsland, M. Smith, D. C. Benner, V. M. Devi, J.-M. Flaud, C. Camy-Peyret, and R. Transfer, "The HITRAN molecular database: editions of 1991 and 1992," J. Quantum Spectrosc. Radiat. Transfer **48**, 469 (1992).
3. L. S. Rothman, C. Rinsland, A. Goldman, S. Massie, D. Edwards, J. Flaud, A. Perrin, C. Camy-Peyret, V. Dana, J. Y. Mandin, J. Schroeder, A. Mccann, R. R. Gamache, R. B. Wattson, K. Yoshino, K. V. Chance, K. W. Jucks, L. R. Brown, V. Nemtchinov, and P. Varanasi, "The HITRAN molecular spectroscopic database and HAWKS (HITRAN atmospheric workstation): 1996 edition," J. Quantum Spectrosc. Radiat. Transfer **60**, 665 (1998).
4. J. E. Bertie and Z. J. A. S. Lan, "Infrared intensities of liquids XX: the intensity of the OH stretching band of liquid water revisited, and the best current values of the optical constants of $H_2O$ at 25 C between 15,000 and 1 $cm^{-1}$," Am. Chem. Soc. **50**, 1047 (1996).
5. S. R. Bowman, W. S. Rabinovich, A. P. Bowman, and B. J. Feldman, "3 μm laser performance of Ho:$YAlO_3$ and Nd,Ho:$YAlO_3$," IEEE J. Quantum Electron. **26**, 403 (1990).
6. T. Sumiyoshi, H. Sekita, T. Arai, S. Sato, M. Ishihara, and M. Kikuchi, "High-power continuous-wave and cascade $Ho^{3+}$:ZBLAN fiber laser and its medical applications," IEEE J. Sel. Top. Quantum Electron. **5**, 936 (1999).
7. S. D. Jackson, "Single-transverse-mode 2.5 W holmium-doped fluoride fiber laser operating at 2.86 μm," Opt. Lett. **29**, 334 (2004).
8. C. Wang, H. Xia, Z. Feng, Z. Zhang, D. Jiang, J. Zhang, Q. Sheng, Q. Tang, S. He, H. Jiang, and B. Chen, "Enhanced emission at 2.85 μm of $Ho^{3+}/Pr^{3+}$ co-doped α-$NaYF_4$ single crystal," Optoelectron. Lett. **12**, 56 (2016).
9. H. Nie, P. Zhang, B. Zhang, K. Yang, L. Zhang, T. Li, S. Zhang, J. Xu, Y. Hang, and J. He, "Diode-end-pumped Ho, Pr:$LiLuF_4$ bulk laser at 2.95 μm," Opt. Lett. **42**, 699 (2017).
10. M. Tempus, W. Luethy, H. Weber, V. Ostroumov, and I. Shcherbakov, "2.79 μm YSGG:Cr:Er laser pumped at 790 nm," IEEE J. Quantum Electron. **30**, 2608 (1994).
11. D. W. Chen, C. L. Fincher, T. S. Rose, F. L. Vernon, and R. A. Fields, "Diode-pumped 1 W continuous-wave Er:YAG 3 μm laser," Opt. Lett. **24**, 385 (1999).
12. X. Zhu and R. Jain, "10-W-level diode-pumped compact 2.78 μm ZBLAN fiber laser," Opt. Lett. **32**, 26 (2007).
13. S. Tokita, M. Murakami, S. Shimizu, M. Hashida, and S. Sakabe, "12 W Q-switched Er:ZBLAN fiber laser at 2.8 μm," Opt. Lett. **36**, 2812 (2011).
14. V. Fortin, M. Bernier, S. T. Bah, and R. Vallee, "30 W fluoride glass all-fiber laser at 2.94 μm," Opt. Lett. **40**, 2882 (2015).
15. W. Yao, H. Uehara, H. Kawase, H. Chen, and R. Yasuhara, "Highly efficient Er:YAP laser with 6.9 W of output power at 2920 nm," Opt. Express **28**, 19000 (2020).
16. T. Li, K. Beil, C. Krankel, C. Brandt, and G. Huber, "Laser performance of highly doped Er:$Lu_2O_3$ at 2.8 μm," in *Advanced Solid-State Photonics* (2012), paper AW5A.6.
17. R. Woodward, M. Majewski, G. Bharathan, D. Hudson, A. Fuerbach, and S. D. Jackson, "Watt-level dysprosium fiber laser at 3.15 μm with 73% slope efficiency," Opt. Lett. **43**, 1471 (2018).
18. S. D. Jackson, "Continuous wave 2.9 μm dysprosium-doped fluoride fiber laser," Appl. Phys. Lett. **83**, 1316 (2003).
19. H. Luo, J. Li, Y. Gao, Y. Xu, X. Li, and Y. Liu, "Tunable passively Q-switched $Dy^{3+}$-doped fiber laser from 2.71 to 3.08 μm using PbS nanoparticles," Opt. Lett. **44**, 2322 (2019).
20. Y. Wang, J. Li, Z. Zhu, Z. You, J. Xu, and C. Tu, "Mid-infrared emission in Dy:$YAlO_3$ crystal," Opt. Mater. Express **4**, 1104 (2014).
21. X. Zhu, G. Zhu, C. Wei, L. V. Kotov, J. Wang, M. Tong, R. A. Norwood, and N. Peyghambarian, "Pulsed fluoride fiber lasers at 3 μm [Invited]," J. Opt. Soc. Am. B **34**, 538 (2017).
22. P. L. Melngailis, "Maser action in InAs diodes," Appl. Phys. Lett. **2**, 176 (1963).
23. D. Garbuzov, H. Lee, V. Khalfin, R. Martinelli, J. Connolly, and T. L. Belenky, "2.3–2.7 μm room temperature CW operation of InGaAsSb-AlGaAsSb broad waveguide SCH-QW diode lasers," IEEE Poton. Technol. Lett. **11**, 794 (1999).
24. A. D. Andreev and D. V. Donetsky, "Analysis of temperature dependence of the threshold current in 2.3–2.6 μm InGaAsSb/AlGaAsSb quantum-well lasers," Appl. Phys. Lett. **74**, 2743 (1999).
25. H. Choi, S. Eglash, and G. J. Turner, "Double-heterostructure diode lasers emitting at 3 μm with a metastable GaInAsSb active layer and AlGaAsSb cladding layers," Appl. Phys. Lett. **64**, 2474 (1994).
26. A. Joullié, P. Christol, A. N. Baranov, and A. J. Vicet, "Mid-Infrared 2–5 μm heterojunction laser diodes," in *Solid-State Mid-Infrared Laser Sources*, (Springer, 2003), Vol. **89**.
27. C. Sirtori and J. J. Nagle, "Quantum cascade lasers: the quantum technology for semiconductor lasers in the mid-far-infrared," C. R. Physique **4**, 639 (2003).
28. D. Hofstetter and M. I. Faist, *High Performance Quantum Cascade Lasers and Their Applications* (Springer Berlin Heidelberg, 2003).
29. G. Soboń, T. Martynkien, P. Mergo, L. Rutkowski, and A. J. Foltynowicz, "High-power frequency comb source tunable from 2.7 to 4.2 μm based on difference frequency generation pumped by an Yb-doped fiber laser," Opt. Lett. **42**, 1748 (2017).
30. J. Zhang, K. Fritsch, Q. Wang, F. Krausz, K. F. Mak, and O. J. Pronin, "Intrapulse difference-frequency generation of mid-infrared (2.7–20 μm) by random quasi-phase-matching," Opt. Lett. **44**, 2986 (2019).
31. L. E. Myers, R. Eckardt, M. Fejer, R. Byer, W. Bosenberg, and J. B. Pierce, "Quasi-phase-matched optical parametric oscillators in bulk periodically poled $LiNbO_3$," J. Opt. Soc. Am. B **12**, 2102 (1995).
32. A. Godard, "Infrared (2–12 μm) solid-state laser sources: a review," Comptes Rendus Physique **8**, 1100 (2007).
33. H. Ishizuki and T. J. Taira, "High-energy quasi-phase-matched optical parametric oscillation in a periodically poled MgO:$LiNbO_3$ device with a 5 mm × 5 mm aperture," Opt. Lett. **30**, 2918 (2005).
34. Y. Peng, X. Wei, X. Luo, Z. Nie, J. Peng, Y. Wang, and D. J. Shen, "High-power and widely tunable mid-infrared optical parametric amplification based on PPMgLN," Opt. Lett. **41**, 49 (2016).
35. H. J. Krause and W. J. Daum, "High-power source of coherent picosecond light pulses tunable from 0.41 to 12.9 μm," Appl. Phys. B **56**, 8 (1993).
36. A. B. Seddon, Z. Tang, D. Furniss, S. Sujecki, and T. M. Benson, "Progress in rare-earth-doped mid-infrared fiber lasers," Opt. Express **18**, 26704 (2010).

37. C. Zhao, Y. Hang, L. Zhang, J. Yin, P. Hu, and E. Ma, "Polarized spectroscopic properties of $Ho^{3+}$-doped $LuLiF_4$ single crystal for 2 μm and 2.9 μm lasers," Opt. Mater. **33**, 1610 (2011).
38. D. D. Hudson, S. D. Jackson, and B. J. Eggleton, "Novel laser sources in the mid-infrared," in *IEEE 3rd International Conference on Photonics* (2012), p. 381.
39. P. Zhang, Y. Hang, and L. Zhang, "Deactivation effects of the lowest excited state of $Ho^{3+}$ at 2.9 μm emission introduced by $Pr^{3+}$ ions in $LiLuF_4$ crystal," Opt. Lett. **37**, 5241 (2012).
40. J. Ma, Z. Qin, G. Xie, L. Qian, and D. Tang, "Review of mid-infrared mode-locked laser sources in the 2.0 μm–3.5 μm spectral region," Appl. Phys. Rev. **6**, 140 (2019).
41. Y. O. Aydın, V. Fortin, F. Maes, F. Jobin, S. D. Jackson, R. Vallée, and M. Bernier, "Diode-pumped mid-infrared fiber laser with 50% slope efficiency," Optica **4**, 235 (2017).
42. R. I. Woodward, M. R. Majewski, G. Bharathan, D. D. Hudson, A. Fuerbach, and S. D. Jackson, "Watt-level dysprosium fiber laser at 3.15 μm with 73% slope efficiency," Opt. Lett. **43**, 1471 (2018).
43. M. Robinson and D. P. Devor, "Thermal switching of laser emission of $Er^{3+}$ at 2.69 μm and $Tm^{3+}$ at 1.86 μm in mixed crystals of $CaF_2$:$ErF_3$:$TmF_3$," Appl. Phys. Lett. **10**, 167 (1967).
44. J. Chen, D. Sun, J. Luo, J. Xiao, H. Kang, H. Zhang, M. Cheng, Q. Zhang, and S. Yin, "Spectroscopic, diode-pumped laser properties and gamma irradiation effect on Yb, Er, Ho:GYSGG crystals," Opt. Lett. **38**, 1218 (2013).
45. V. Lupei, S. Georgescu, and V. Florea, "On the dynamics of population inversion for 3 μm $Er^{3+}$ lasers," IEEE J. Quantum Electron. **29**, 426 (1993).
46. B. J. Dinerman and P. F. Moulton, "3-μm cw laser operations in erbium-doped YSGG, GGG, and YAG," Opt. Lett. **19**, 1143 (1994).
47. T. Jensen, V. G. Ostroumov, and G. Huber, "Upconversion processes in $Er^{3+}$: YSGG and diode-pumped laser experiments at 2.8 μm," in *Advanced Solid State Lasers* (1995), paper IL4.
48. C. Wyss, W. Lüthy, H. P. Weber, P. Rogin, and J. Hulliger, "Emission properties of an optimised 2.8 μm $Er^{3+}$:YLF laser," Opt. Commun. **139**, 215 (1997).
49. T. Li, K. Beil, C. Kränkel, and G. Huber, "Efficient high-power continuous wave Er:$Lu_2O_3$ laser at 2.85 μm," Opt. Lett. **37**, 2568 (2012).
50. Y. Wang, Z. You, J. Li, and Z. Zhu, En, and C. Tu, "Spectroscopic investigations of highly doped $Er^{3+}$:GGGG and $Er^{3+}$/$Pr^{3+}$:GGGG crystals," J. Phys. D **42**, 215406 (2009).
51. H. Zhang, X. Meng, C. Wang, P. Wang, L. Zhu, X. Liu, C. Dong, Y. Yang, R. Cheng, J. Dawes, J. Piper, S. Zhang, and L. Sun, "Growth, spectroscopic properties and laser output of Er:$Ca_4YO(BO_3)_3$ and Er:Yb:$Ca_4YO(BO_3)_3$ crystals," J. Crystal Growth **218**, 81 (2000).
52. Y. D. Zavartsev, A. I. Zagumennyi, L. A. Kulevskii, A. V. Lukashev, P. P. Pashinin, P. A. Studenikin, I. A. Shcherbakov, and A. F. Umyskov, "*Q*-switching in a $Cr^{3+}$: $Yb^{3+}$: $Ho^{3+}$: YSGG crystal laser based on the $^5I_6$–$^5I_7$ ($\lambda$ = 2.92 μm) transition," Quantum Electron. **29**, 295 (1999).
53. F. H. Jagosich, L. Gomes, L. V. G. Tarelho, L. C. Courrol, and I. M. Ranieri, "Deactivation effects of the lowest excited states of $Er^{3+}$ and $Ho^{3+}$ introduced by $Nd^{3+}$ ions in $LiYF_4$ crystals," J. Appl. Phys. **91**, 624 (2002).
54. J. Hu, H. Xia, H. Hu, X. Zhuang, Y. Zhang, H. Jiang, and B. Chen, "Enhanced 2.7 μm emission from diode-pumped $Er^{3+}$/$Pr^{3+}$ co-doped $LiYF_4$ single crystal grown by Bridgman method," Mater. Res. Bull. **48**, 2604 (2013).
55. X. Zhuang, H. Xia, H. Hu, J. Hu, P. Wang, J. Peng, Y. Zhang, H. Jiang, and B. Chen, "Enhanced emission of 2.7 μm from $Er^{3+}$/$Nd^{3+}$-codoped $LiYF_4$ single crystals," Mater. Sci. Eng. B **178**, 326 (2013).
56. P. Wang, H. Xia, J. Peng, H. Hu, L. Tang, Y. Zhang, B. Chen, and H. Jiang, "Concentration effect of $Nd^{3+}$ ion on the spectroscopic properties of $Er^{3+}$/$Nd^{3+}$ co-doped $LiYF_4$ single crystal," Mater. Chem. Phys. **144**, 349 (2014).
57. Z. You, Y. Wang, J. Xu, Z. Zhu, J. Li, and C. Tu, "Diode-end-pumped mid-infrared multiwavelength Er: Pr: GGG laser," IEEE Photon. Technol. Lett. **26**, 667 (2014).
58. J. Liu, X. Fan, J. Liu, W. Ma, J. Wang, and L. Su, "Mid-infrared self-*Q*-switched Er, Pr:$CaF_2$ diode-pumped laser," Opt. Lett. **41**, 4660 (2016).
59. H. Xia, J. Feng, Y. Ji, Y. Sun, Y. Wang, Z. Jia, and C. Tu, "2.7 μm emission properties of $Er^{3+}$/$Yb^{3+}$/$Eu^{3+}$:$SrGdGa_3O_7$ and $Er^{3+}$/$Yb^{3+}$/$Ho^{3+}$:$SrGdGa_3O_7$ crystals," J. Quant. Spectrosc. Radiat. Transfer **173**, 7 (2016).
60. X. Zhao, D. Sun, J. Luo, H. Zhang, Z. Fang, C. Quan, L. Hu, M. Cheng, Q. Zhang, and S. Yin, "Laser performance of a 966 nm LD side-pumped Er,Pr:GYSGG laser crystal operated at 2.79 μm," Opt. Lett. **43**, 4312 (2018).
61. B. J. Dinerman, C. L. Moulton, and A. Pinto, "CW laser operation from Er: YAG, Er:GGG and Er:YSGG," in *Advanced Solid State Lasers* (1992), paper ML10.
62. R. C. Stoneman and L. Esterowitz, "Efficient resonantly pumped 2.8 μm $Er^{3+}$: GSGG laser," Opt. Lett. **17**, 816 (1992).
63. A. Gallian, A. Martinez, P. Marine, V. Fedorov, S. Mirov, V. Badikov, D. Boutoussov, and M. Andriasyan, "Fe:ZnSe passive *Q*-switching of 2.8 μm Er:Cr:YSGG laser cavity," Proc. SPIE **6451**, 64510L (2007).
64. J. Luo, D. Sun, H. Zhang, Q. Guo, Z. Fang, X. Zhao, M. Cheng, Q. Zhang, and S. Yin, "Growth, spectroscopy, and laser performance of a 2.79 μm Cr,Er,Pr: GYSGG radiation-resistant crystal," Opt. Lett. **40**, 4194 (2015).
65. X. Zhao, D. Sun, J. Luo, H. Zhang, C. Quan, L. Hu, Z. Han, K. Dong, M. Cheng, and S. Yin, "Spectroscopic and laser properties of Er:LuSGG crystal for high-power approximately 2.8 μm mid-infrared laser," Opt. Express **28**, 8843 (2020).
66. W. Q. Shi, R. Kurtz, J. Machan, M. Bass, M. Birnbaum, and M. Kokta, "Simultaneous, multiple wavelength lasing of (Er, Nd):$Y_3Al_5O_{12}$," Appl. Phys. Lett. **51**, 1218 (1987).
67. Q. Hu, H. Nie, W. Mu, Y. Yin, J. Zhang, B. Zhang, J. He, Z. Jia, and X. Tao, "Bulk growth and an efficient mid-IR laser of high-quality Er:YSGG crystals," Crystengcomm **21**, 1928 (2019).
68. R. Stoneman, J. Lynn, and L. Esterowitz, "Direct upper-state pumping of the 2.8 μm, $Er^{3+}$:YLF laser," IEEE J. Quantum Electron. **28**, 1041 (1992).
69. C. Labbe, J. Doualan, P. Camy, R. Moncorgé, and M. Thuau, "The 2.8 μm laser properties of $Er^{3+}$ doped $CaF_2$ crystals," Opt. Commun. **209**, 193 (2002).
70. T. T. Basiev, Y. V. Orlovskii, M. V. Polyachenkova, P. P. Fedorov, S. V. Kuznetsov, V. A. Konyushkin, V. V. Osiko, O. K. Alimov, and A. Y. Dergachev, "Continuously tunable cw lasing near 2.75 μm in diode-pumped $Er^{3+}$:$SrF_2$ and $Er^{3+}$:$CaF_2$ crystals," Quantum Electron. **36**, 591 (2006).
71. J. Liu, X. Feng, X. Fan, Z. Zhang, B. Zhang, J. Liu, and L. Su, "Efficient continuous-wave and passive *Q*-switched mode-locked $Er^{3+}$:$CaF_2$-$SrF_2$ lasers in the mid-infrared region," Opt. Lett. **43**, 2418 (2018).
72. R. Švejkar, J. Šulc, H. Jelínková, V. Kubeček, W. Ma, D. Jiang, Q. Wu, and L. Su, "Diode-pumped Er:$SrF_2$ laser tunable at 2.7 μm," Opt. Mater. Express **8**, 1025 (2018).
73. C. Quan, D. Sun, J. Luo, H. Zhang, Z. Fang, X. Zhao, L. Hu, M. Cheng, Q. Zhang, and S. Yin, "2.7 μm dual-wavelength laser performance of LD end-pumped Er:YAP crystal," Opt. Express **26**, 28421 (2018).
74. H. Kawase and R. Yasuhara, "2.92-μm high-efficiency continuous-wave laser operation of diode-pumped Er:YAP crystal at room temperature," Opt. Express **27**, 12213 (2019).
75. L. Merkle, N. Ter-Gabrielyan, and V. Fromzel, "Cryogenic laser properties of Er:YAG and Er:$Sc_2O_3$-a comparison," in *Advanced Solid-State Photonics* (2011), paper AWA2.
76. L. Wang, H. Huang, D. Shen, J. Zhang, H. Chen, Y. Wang, X. Liu, and D. Tang, "Room temperature continuous-wave laser performance of LD pumped Er:$Lu_2O_3$ and Er:$Y_2O_3$ ceramic at 2.7 μm," Opt. Express **22**, 19495 (2014).
77. H. Uehara, R. Yasuhara, S. Tokita, J. Kawanaka, M. Murakami, and S. Shimizu, "Efficient continuous wave and quasi-continuous wave operation of a 2.8 μm Er:$Lu_2O_3$ ceramic laser," Opt. Express **25**, 18677 (2017).
78. X. Guan, J. Wang, Y. Zhang, B. Xu, Z. Luo, H. Xu, Z. Cai, X. Xu, J. Zhang, and J. Xu, "Self-*Q*-switched and wavelength-tunable tungsten disulfide-based passively *Q*-switched Er:$Y_2O_3$ ceramic lasers," Photon. Res. **6**, 830 (2018).
79. D. Yin, J. Wang, Y. Wang, P. Liu, J. Ma, X. Xu, D. Shen, Z. Dong, L. B. Kong, and D. Tang, "Fabrication of Er:$Y_2O_3$ transparent ceramics for 2.7 μm mid-infrared solid-state lasers," J. Euro. Ceram. Soc. **40**, 444 (2019).
80. Y. O. Aydın, V. Fortin, F. Maes, F. Jobin, S. D. Jackson, R. Vallée, and M. Bernier, "Diode-pumped mid-infrared fiber laser with 50% slope efficiency," Optica **4**, 235 (2017).
81. N. Ter-Gabrielyan and V. Fromzel, "Cascade generation at 1.62, 1.73 and 2.8 μm in the Er:YLF *Q*-switched laser," Opt. Express **27**, 20199 (2019).
82. G. S. John, W. David, and F. Josh, "Efficient 1.5 W CW and 9 mJ quasi-CW $TEM_{00}$ mode operation of a compact diode-laser-pumped 2.94 μm Er:YAG laser," Proc. SPIE **7578**, 75781E (2010).
83. B. Shen, H. Kang, P. Chen, J. Liang, Q. Ma, J. Fang, D. Sun, Q. Zhang, S. Yin, X. Yan, and L. Gao, "Performance of continuous-wave laser-diode side-pumped Er:YSGG slab lasers at 2.79 μm," Appl. Phys. B **121**, 511 (2015).

84. L. You, D. Lu, Z. Pan, H. Yu, H. Zhang, and J. Wang, "High-efficiency 3 μm Er:YGG crystal lasers," Opt. Lett. **43**, 5873 (2018).
85. H. Xue, L. Wang, W. Zhou, H. Wang, J. Wang, D. Tang, and D. Shen, "Stable *Q*-switched mode-locking of 2.7 μm Er:$Y_2O_3$ ceramic laser using a semiconductor saturable absorber," Appl. Sci. **8**, 1155 (2018).
86. Z. D. Fleischman and T. Sanamyan, "Spectroscopic analysis of $Er^{3+}$:$Y_2O_3$ relevant to 27 μm mid-IR laser," Opt. Mater. Express **6**, 3109 (2016).
87. T. Sanamyan and M. Dubinskii, "$Er^{3+}$-doped diode-pumped ceramic laser delivers 14 W CW at 2.7 μm," in *CLEO* (2011), paper CMY1.
88. W. Yao, H. Uehara, S. Tokita, H. Chen, D. Konishi, M. Murakami, and R. Yasuhara, "LD-pumped 2.8 μm Er:$Lu_2O_3$ ceramic laser with 6.7 W output power and >30% slope efficiency," Appl. Phys. Express **14**, 012001 (2020).
89. H. Kawase, H. Uehara, H. Chen, and R. Yasuhara, "Passively *Q*-switched 2.9 μm Er:YAP single crystal laser using graphene saturable absorber," Appl. Phys. Express **12**, 102006 (2019).
90. J. Chen, D. Sun, J. Luo, H. Zhang, R. Dou, J. Xiao, Q. Zhang, and S. Yin, "Spectroscopic properties and diode end-pumped 2.79 μm laser performance of Er,Pr:GYSGG crystal," Opt. Express **21**, 23425 (2013).
91. M. Inochkin, L. Khloponin, V. Khramov, G. Altshuler, A. Erofeev, S. Wilson, and F. Feldchein, "High-efficiency diode-pumped Er:YLF laser with multi-wavelength generation," Proc. SPIE **8235**, 823502 (2012).
92. S. Wüthrich, W. Lüthy, and H. P. Weber, "Comparison of YAG:Er and $YAlO_3$:Er laser crystals emitting near 2.9 μm," J. Appl. Phys. **68**, 5467 (1990).
93. A. Zajac, M. Skorczakowski, J. Swiderski, and P. Nyga, "Electrooptically *Q*-switched mid-infrared Er:YAG laser for medical applications," Opt. Express **12**, 5125 (2004).
94. P. Koranda, H. Jelínková, M. Nemec, J. Sulc, and M. Cech, "Electro-optically Q-switched Er:YAG laser," in *Lasers and Applications in Science and Engineering* (2005), p. 141.
95. V. A. Akimov, M. P. Frolov, Y. V. Korostelin, V. I. Kozlovsky, A. I. Landman, Y. P. Podmar'kov, V. G. Polushkin, and A. A. Voronov, "2.94 μm Er:YAG *Q*-switched laser with $FE^{2+}$:ZnSe passive shutter," Proc. SPIE **6610**, 661008 (2007).
96. L. Wang, J. Wang, J. Yang, X. Wu, D. Sun, S. Yin, H. Jiang, J. Wang, and C. Xu, "2.79 μm high peak power LGS electro-optically *Q*-switched Cr,Er:YSGG laser," Opt. Lett. **38**, 2150 (2013).
97. J. Wang, T. Cheng, L. Wang, J. Yang, D. Sun, S. Yin, X. Wu, and H. Jiang, "Compensation of strong thermal lensing in an LD side-pumped high-power Er:YSGG laser," Laser Phys. Lett. **12**, 105004 (2015).
98. Z. Qin, G. Xie, J. Zhang, J. Ma, P. Yuan, and L. Qian, "Continuous-wave and passively *Q*-switched Er:$Y_2O_3$ ceramic laser at 2.7 μm," International J. Opt. **2018**, 3153614 (2018).
99. Y. Zhang, B. Xu, Q. Tian, Z. Luo, H. Xu, Z. Cai, D. Sun, Q. Zhang, P. Liu, X. Xu, and J. Zhang, "Sub-15-ns passively *Q*-switched Er:YSGG laser at 2.8 μm with Fe:ZnSe saturable absorber," IEEE Photon. Technol. Lett. **31**, 565 (2019).
100. Q. Bao, H. Zhang, Y. Wang, Z. Ni, Y. Yan, Z. X. Shen, K. P. Loh, and D. Y. Tang, "Atomic-layer graphene as a saturable absorber for ultrafast pulsed lasers," Adv. Funct. Mater. **19**, 3077 (2009).
101. Z. You, Y. Sun, D. Sun, Z. Zhu, Y. Wang, J. Li, C. Tu, and J. Xu, "High performance of a passively *Q*-switched mid-infrared laser with $Bi_2Te_3$/graphene composite SA," Opt. Lett. **42**, 871 (2017).
102. X. Su, H. Nie, Y. Wang, G. Li, B. Yan, B. Zhang, K. Yang, and J. He, "Few-layered $ReS_2$ as saturable absorber for 2.8 μm solid state laser," Opt. Lett. **42**, 3502 (2017).
103. J. Liu, H. Huang, F. Zhang, Z. Zhang, J. Liu, H. Zhang, and L. Su, "Bismuth nanosheets as a *Q*-switcher for a mid-infrared erbium-doped $SrF_2$ laser," Photon. Res. **6**, 762 (2018).
104. Q. Hao, J. Liu, Z. Zhang, B. Zhang, F. Zhang, J. Yang, J. Liu, L. Su, and H. Zhang, "Mid-infrared Er:$CaF_2$–$SrF_2$ bulk laser *Q*-switched by MXene $Ti_3C_2T_x$ absorber," Appl. Phys. Express **12**, 085506 (2019).
105. J. Liu, J. Liu, Z. Guo, H. Zhang, W. Ma, J. Wang, and L. Su, "Dual-wavelength *Q*-switched Er:$SrF_2$ laser with a black phosphorus absorber in the mid-infrared region," Opt. Express **24**, 30289 (2016).
106. M. Fan, T. Li, S. Zhao, G. Li, H. Ma, X. Gao, C. Kränkel, and G. Huber, "Watt-level passively *Q*-switched Er:$Lu_2O_3$ laser at 2.84 μm using $MoS_2$," Opt. Lett. **41**, 540 (2016).
107. J. Xu, M. Li, and Y. J. L. P. Chen, "$WS_2$ passively *Q*-switched Er:$SrF_2$ laser at ~3 μm," Laser Phys. **29**, 055802 (2019).
108. Y. Yao, N. Cui, Q. Wang, L. Dong, and J. L. He, "Highly efficient continuous-wave and $ReSe_2$ *Q*-switched 3 μm dual-wavelength Er:YAP crystal lasers," Opt. Lett. **44**, 2839 (2019).
109. B. Yan, B. Zhang, H. Nie, G. Li, X. Sun, Y. Wang, J. Liu, B. Shi, S. Liu, and J. He, "Broadband 1T-titanium selenide-based saturable absorbers for solid-state bulk lasers," Nanoscale **10**, 20171 (2018).
110. X. Guan, L. Zhan, Z. Zhu, B. Xu, H. Xu, Z. Cai, W. Cai, X. Xu, J. Zhang, and J. Xu, "Continuous-wave and chemical vapor deposition graphene-based passively *Q*-switched Er:$Y_2O_3$ ceramic lasers at 2.7 μm," Appl. Opt. **57**, 371 (2018).
111. P. Tang, Z. Qin, J. Liu, C. Zhao, G. Xie, S. Wen, and L. Qian, "Watt-level passively mode-locked $Er^{3+}$-doped ZBLAN fiber laser at 2.8 μm," Opt. Lett. **40**, 4855 (2015).
112. R. I. Woodward, D. D. Hudson, A. Fuerbach, and S. D. Jackson, "Generation of 70 fs pulses at 2.86 μm from a mid-infrared fiber laser," Opt. Lett. **42**, 4893 (2017).
113. H. Gu, Z. Qin, G. Xie, T. Hai, P. Yuan, J. Ma, and L. Qian, "Generation of 131 fs mode-locked pulses from 2.8 μm Er:ZBLAN fiber laser," Chin. Opt. Lett. **18**, 031402 (2020).
114. C. Wei, X. Zhu, R. A. Norwood, and N. Peyghambarian, "Passively continuous-wave mode-locked $Er^{3+}$-doped ZBLAN fiber laser at 2.8 μm," Opt. Lett. **37**, 3849 (2012).
115. X. Zhu, G. Zhu, C. Wei, L. V. Kotov, J. Wang, M. Tong, R. A. Norwood, and N. Peyghambarian, "Pulsed fluoride fiber lasers at 3 μm [Invited]," J. Opt. Soc. Am. B **34**, A15 (2017).
116. H. Luo, J. Yang, J. Li, and Y. Liu, "Tunable sub-300 fs soliton and switchable dual-wavelength pulse generation from a mode-locked fiber oscillator around 2.8 μm," Opt. Lett. **46**, 841 (2021).
117. J. Machan, R. Kurtz, M. Bass, M. Birnbaum, and M. Kokta, "Simultaneous, multiple wavelength lasing of (Ho, Nd):$Y_3Al_5O_{12}$," Appl. Phys. Lett. **51**, 1313 (1987).
118. A. F. Umyskov, D. Z. Yu, A. I. Zagumennyi, V. O. Vyacheslav, and P. A. Studenikin, "$Cr^{3+}$, $Yb^{3+}$, $Ho^{3+}$:YSGG crystal laser with a continuously tunable emission wavelength in the range 2.84–3.05 μm," Quantum Electron. **26**, 563 (1996).
119. A. Diening and S. Kuck, "Spectroscopy and diode-pumped laser oscillation of $Yb^{3+}$, $Ho^{3+}$-doped yttrium scandium gallium garnet," J. Appl. Phys. **87**, 4063 (2000).
120. Z. Wang, B. Zhang, J. He, K. Yang, K. Han, J. Ning, J. Hou, and F. Lou, "Passively *Q*-switched mode-locking of Tm:YAP laser based on Cr:ZnS saturable absorber," Appl. Opt. **54**, 4333 (2015).
121. J. Q. Hong, L. H. Zhang, M. Xu, and Y. Hang, "Activation and deactivation effects to $Ho^{3+}$ at ~2.8 μm MIR emission by $Yb^{3+}$ and $Pr^{3+}$ ions in YAG crystal," Opt. Mater. Express **6**, 1444 (2016).
122. H. Zhang, X. Sun, J. Luo, Z. Fang, X. Zhao, M. Cheng, Q. Zhang, and D. Sun, "Structure, defects, and spectroscopic properties of a Yb,Ho,Pr:YAP laser crystal," J. Alloys Comp. **672**, 223 (2016).
123. J. Hong, L. Zhang, and Y. Hang, "Enhanced 2.86 μm emission of $Ho^{3+}$,$Pr^{3+}$-codoped $LaF_3$ single crystal," Opt. Mater. Express **7**, 1509 (2017).
124. S. Li, L. Zhang, M. He, G. Chen, Y. Yang, S. Zhang, M. Xu, T. Yan, N. Ye, and Y. Hang, "$Nd^{3+}$ as effective sensitizing and deactivating ions for the 2.87 μm lasers in $Ho^{3+}$ doped $LaF_3$ crystal," J. Lumin. **208**, 63 (2019).
125. S. Wang, J. Zhang, N. Xu, S. Jia, G. Brambilla, and P. Wang, "2.9 μm lasing from a $Ho^{3+}$/$Pr^{3+}$ co-doped $AlF_3$-based glass fiber pumped by a 1150 nm laser," Opt. Lett. **45**, 1216 (2020).
126. D. Anthon and T. Pier, "Laser-pumped 3 μm Ho:YAG and Ho:GGG lasers," in *Advanced Solid State Lasers* (1990), paper MML3.
127. A. F. Umyskov, Y. D. Zavartsev, A. I. Zagumennyi, V. V. Osiko, and P. A. Studenikin, "Efficient 3 μm $Cr^{3+}$:$Yb^{3+}$:$Ho^{3+}$:YSGG crystal laser," Quantum Electron. **26**, 771 (1996).
128. A. V. Lukashev, Y. D. Zavartsev, A. I. Zagumennyi, M. E. Karasev, L. A. Kulevskii, P. P. Pashinin, P. A. Studenikin, and V. N. Tranev, "Efficient flash lamp pumped YSGG:Cr:Yb:Ho laser at 3 μm," in *IEEE LEOS Annual Meeting Conference* (1999), p. 914
129. A. Diening, E. A. Möbert, E. Heumann, G. Huber, and B. H. T. Chai, "Diode-pumped cw lasing of Yb,Ho:$KYF_4$ in the 3 μm spectral range in comparison to Er:$KYF_4$," Laser Phys. **8**, 214 (1998).

130. H. Nie, P. Zhang, B. Zhang, M. Xu, K. Yang, X. Sun, L. Zhang, Y. Hang, and J. He, "Watt-level continuous-wave and black phosphorus passive *Q*-switching operation of $Ho^{3+}$,$Pr^{3+}$:$LiLuF_4$ bulk laser at 2.95 μm," IEEE J. Sel. Top. Quantum Electron. **53**, 8400208 (2017).
131. H. Nie, H. Xia, B. Shi, J. Hu, B. Zhang, K. Yang, and J. He, "High-efficiency watt-level continuous-wave 2.9 μm Ho,Pr:YLF laser," Opt. Lett. **43**, 6109 (2018).
132. H. Nie, B. Shi, H. Xia, J. Hu, B. Zhang, K. Yang, and J. L. He, "High-repetition-rate kHz electro-optically *Q*-switched Ho, Pr:YLF 2.9 μm bulk laser," Opt. Express **26**, 33671 (2018).
133. S. Bowman, W. Rabinovich, A. Bowman, B. Feldman, and G. Rosenblatt, "3 μm laser performance of Ho:$YAlO_3$ and Nd, Ho:$YAlO_3$," IEEE J. Quantum Electron. **26**, 403 (1990).
134. S. Bowman, W. Rabinovich, B. Feldman, and M. Winings, "Tuning the 3 μm Ho:$YAlO_3$ Laser," in *Advanced Solid State Lasers* (1990), paper MML4.
135. H. Nie, P. Zhang, B. Zhang, M. Xu, K. Yang, X. Sun, L. Zhang, Y. Hang, and J. He, "Watt-level continuous-wave and black phosphorus passive *Q*-switching operation of $Ho^{3+}$,$Pr^{3+}$:$LiLuF_4$ bulk laser at 2.95 μm," IEEE J. Sel. Top. Quantum Electron. **24**, 1600205 (2017).
136. Z. Yan, G. Li, T. Li, S. Zhao, K. Yang, S. Zhang, M. Fan, L. Guo, and B. Zhang, "Passively *Q*-switched Ho,Pr:$LiLuF_4$ laser at 2.95 μm using $MoSe_2$," IEEE Photon. J. **9**, 1506207 (2017).
137. H. Nie, X. Sun, B. Zhang, B. Yan, G. Li, Y. Wang, J. Liu, B. Shi, S. Liu, and J. He, "Few-layer $TiSe_2$ as a saturable absorber for nanosecond pulse generation in 2.95 μm bulk laser," Opt. Lett. **43**, 3349 (2018).
138. M. Fan, T. Li, G. Li, S. Zhao, K. Yang, S. Zhang, B. Zhang, J. Xu, and C. Kränkel, "Passively *Q*-switched Ho,Pr:$LiLuF_4$ laser with graphitic carbon nitride nanosheet film," Opt. Express **25**, 12796 (2017).
139. W. Duan, H. Nie, X. Sun, B. Zhang, G. He, Q. Yang, H. Xia, R. Wang, J. Zhan, and J. He, "Passively *Q*-switched mid-infrared laser pulse generation with gold nanospheres as a saturable absorber," Opt. Lett. **43**, 1179 (2018).
140. S. Liu, H. Nie, B. Zhang, S. Li, Y. Yan, and L. He, "Continuous-wave-tunable and passively *Q*-switched 2.9 μm Ho,Pr:$LiLuF_4$ lasers," Laser Phys. Lett. **16**, 015802 (2019).
141. L. F. Johnson and H. J. Guggenheim, "Laser emission at 3 μm from $Dy^{3+}$ in $BaY_2F_8$," Appl. Phys. Lett. **23**, 96 (1973).
142. N. Djeu, V. E. Hartwell, A. A. Kaminskii, and A. V. Butashin, "Room-temperature 3.4 μm Dy:$BaYb_2F_8$ laser," Opt. Lett. **22**, 997 (1997).
143. Y. H. Tsang and A. E. El, "Efficient 2.96 μm dysprosium-doped fluoride fibre laser pumped with a Nd: YAG laser operating at 1.3 μm," Opt. Express **14**, 678 (2006).
144. M. R. Majewski and S. D. Jackson, "Highly efficient mid-infrared dysprosium fiber laser," Opt. Lett. **41**, 2173 (2016).
145. R. I. Woodward, M. R. Majewski, N. Macadam, G. Hu, T. Albrow-Owen, T. Hasan, and S. D. Jackson, "*Q*-switched Dy:ZBLAN fiber lasers beyond 3 μm: comparison of pulse generation using acousto-optic modulation and inkjet-printed black phosphorus," Opt. Express **27**, 15032 (2019).
146. H. Luo, Y. Xu, J. Li, and Y. Liu, "Gain-switched dysprosium fiber laser tunable from 2.8 to 3.1 μm," Opt. Express **27**, 27151 (2019).
147. Y. Dwivedi and S. B. Rai, "Spectroscopic study of $Dy^{3+}$ and $Dy^{3+}$/$Yb^{3+}$ ions co-doped in barium fluoroborate glass," Opt. Mater. **31**, 1472 (2009).
148. P. Zhang, M. Xu, L. Zhang, J. Hong, X. Wang, Y. Wang, G. Chen, and Y. Hang, "Intense 2.89 μm emission from $Dy^{3+}$/$Yb^{3+}$-codoped $PbF_2$ crystal by 970 nm laser diode pumping," Opt. Express **23**, 27786 (2015).